of 8.7 km, but the important fact is that high-velocity material ($\geqslant 4000$ m/sec) must lie beneath the 1200-m/sec material. The 1200-m/sec material is 925 m thick and it is overlain by a layer with a thickness of 248 m and a velocity of 250 m/sec.

Our results have shown that, at least beneath the Taurus-Littrow site, the seismic velocity increases in a stepwise manner in the upper several kilometers. It is of interest to examine our in situ velocity information in the light of the surface geological investigations at the Apollo 17 site, laboratory velocity measurements from returned lunar samples, and seismic velocity measurements on terrestrial lunar analogs.

Premission analyses have shown that much of the Apollo 17 landing site area is covered by a dark mantling material. Observations by the Apollo 17 crew on the lunar surface revealed that any boundary between an overlying thin regolith and the dark mantling material was not readily discernible. Because our closest distance between an explosive charge and the receiver was about 100 m we could not resolve the properties of the upper 20 m or so, and cannot determine whether the interface between the dark mantling material and the subfloor represents a sharp seismic discontinuity or is gradational. However, our data indicate that any horizon, if present, would be less than 20 m from the lunar surface.

Underlying the dark mantling material the dominant rock type observed by the Apollo 17 crew is a medium-grained vesicular basalt believed to be primarily mare-type basalt. Observations in crater walls revealed textural variations, suggesting that individual flow units are involved. Our seismic observations have indicated 248 m of 250-m/sec material overlying 925 m of 1200-m/sec material.

The abrupt change in seismic velocity (and, by inference, in other physical properties) from 250 to 1200 m/sec is suggestive of a major change in the nature of the evolution or deposition of the Apollo 17 subfloor basalts. However, a similar range of seismic velocities is observed with refraction surveys in lava flows on the earth (*5*).

The velocities observed in terrestrial lava flows bracket the velocities measured at the Apollo 17 site and therefore support the presence of lava flows in the Taurus-Littrow valley. Whether the velocity of 250 m/sec is representative of a separate flow or several flows separated by lower-velocity layers of ash or ejecta cannot be resolved from the seismic data. Individual flows may be fractured or brecciated, which could further decrease their seismic velocities. Surface layers of fractured loose blocky material merging into more welded flows are common occurrences on the earth. We believe that the total thickness of the materials with seismic velocities of 250 and 1200 m/sec (1173 m) represents the full thickness of the subfloor basalts at the Apollo 17 site (*6*).

The nature of the 4000-m/sec material underlying the basalts is difficult to unambiguously assign to any particular rock type. It seems likely, based on the geological evidence, that the highland massif material which rings the narrow graben-like valley at the Apollo 17 site underlies the basalt flow or flows. Several rock types were recognized in North Massif and South Massif but the dominant rock type is apparently a coherent breccia believed to be similar to breccias sampled at the Apennine front (Apollo 15) and Descartes (Apollo 16).

Laboratory velocity measurements have been reported for two Apollo 15 breccias, 15418 and 15015 (*7*). Sample 15418 is described as a dark grey breccia of chemical composition similar to anorthite-rich gabbro. Sample 15015 is a more friable breccia of unknown composition. The in situ value of approximately 4000 m/sec is close to the values measured in the laboratory for sample 15015.

Before the Apollo 17 mission the question of how the *P*-wave velocity increased from 100 to 300 m/sec near the surface to about 6 km/sec at a depth of 15 to 20 km was most uncertain. The Apollo 17 lunar seismic profiling results (Fig. 2) have demonstrated that the seismic velocity increases in a sharp stepwise manner in the upper 2.5 km. When our Apollo 17 results are combined with earlier travel time data for direct and surface-reflected arrivals from earlier LM and Saturn (S-IV B) impacts it will be possible to construct a velocity model for the upper lunar crust representative for a lunar mare basin.

ROBERT L. KOVACH
Department of Geophysics, Stanford University, Stanford, California 94305
JOEL S. WATKINS
Marine Biomedical Institute, University of Texas, Galveston 77550

References and Notes

1. R. L. Kovach and J. S. Watkins, *Moon*, in press.
2. H. Kanamori, A. Nur, D. H. Chung, D. Wones, G. Simmons, *Science* **167**, 726 (1970); H. Kanamori, H. Mizutani, Y. Yamano, *Geochim. Cosmochim. Acta* **2** (Suppl. 2), 2323 (1971); N. Warren, E. Schreiber, C. Scholz, J. A. Morrison, P. R. Norton, M. Kumazawa, O. L. Anderson, *ibid.*, p. 2345; O. L. Anderson, C. Scholz, N. Soga, N. Warren, E. Schrieber, *ibid.* **2** (Suppl. 1), 1959 (1970); H. Mizutani, N. Fujii, Y. Hamano, M. Osako, H. Kanamori, in *Revised Abstracts of the Third Lunar Science Conference* (Lunar Science Institute, Houston, 1972), p. 547; P. Talwani, A. Nur, R. L. Kovach, *J. Geophys. Res.*, in press.
3. G. Latham *et al.*, *NASA Spec. Publ. NASA SP-272* (1971), p. 133.
4. G. Latham *et al.*, *NASA Spec. Publ. NASA SP-315* (1973), p. 9-1.
5. J. S. Watkins, L. A. Walters, R. A. Godson, *Geophysics* **37**, 29 (1972).
6. The traverse gravimeter experiment carried out on the Apollo 17 mission suggests basalt flows with a positive density contrast of 0.8 g/cm^3 and a thickness of 1 km (M. Talwani, personal communication).
7. T. Todd, H. Wang, W. S. Baldridge, G. Simmons, *Geochim. Cosmochim. Acta* **3** (Suppl. 3), 2577 (1972).
8. We thank A. Nur for reviewing the manuscript. Supported by NASA contract NAS-9-5632.

6 March 1973

■

Condensation Nucleus Discriminator Making Optical Measurements on Fog: A Tool for Environmental Research

Abstract. *An instrument providing a new, rapid, and accurate method of determining the number and critical radii of condensation nuclei with radii under 200 angstroms is described. Based on the principle of the cloud chamber, the instrument measures transient changes in the attenuation and scattering of a monochromatic light beam by the growing fog droplets. From data obtained the absolute number concentration and radii of condensation nuclei can be calculated. Preliminary studies of aerosol formation in beta-irradiated mixtures of air and sulfur dioxide showed that carbon monoxide and methane inhibit the formation of nuclei; relative rate constants can be deduced. Some applications of this instrument for environmental and basic research are pointed out.*

Condensation nuclei spewed out by factories, homes, and automobiles, as well as by the land and the sea, help to create smog and fog. The importance of condensation nuclei in the environment has been discussed by Shaefer (*1*), who pointed out that removal of visible smoke from a chimney or a jet or automobile exhaust does not mean removal of the pollutant. A worse condition may exist because vaporizing a particle 50 μm in diameter produces about 15 million particles 0.2 μm in diameter. The large hygroscopic particles are easily washed out or fall out by gravity, but the smaller particles are much more resistant to this removal mechanism. Added to this particulate load in the troposphere are the tiny (0.1 to 0.001 μm) Aitken or condensation nuclei created by conversion of gas to particles either at the pollutant source or by reactions initiated in the air. Under normal atmospheric conditions these condensation nuclei do not form visible fog droplets. However, under artificially produced high supersaturation of the air, as in the cloud chamber, they rapidly grow to several micrometers and can be studied by measuring light scattering and attenuation after expansion. This is the principle on which most condensation nucleus counters are based (*2–4*). For size analysis with these instruments, a series of different expansions has to be carried out.

In this report we discuss a useful improvement over the conventional cloud chamber techniques. We record the transient changes in the attenuation and scattering of a monochromatic light beam by the growing fog droplets during an expansion period of 1 to 2 seconds. From a single such recording, the absolute number concentration of condensation nuclei and their critical radii may be derived. Figure 1 is a schematic diagram of the apparatus.

The gas sample, together with a predetermined amount of water vapor and (if desired) filtered tank air for dilution, is introduced into an evacuated reactor flask. For photochemical production of nuclei, the gas sample can be irradiated through a silica window. A ground glass connection (not shown) is available for the insertion of sources of ionizing radiation. The gas pressure in the reactor is monitored by a pressure transducer.

The expansion period is initiated by a timing circuit, which opens a solenoid valve connecting the reactor to an evacuated expansion flask for a predetermined time, up to 2 seconds. Because of the ensuing adiabatic temperature drop and supersaturation, the vapor condenses on the nuclei present, beginning with those having the largest radii and progressing to smaller ones. When the growing droplets reach a radius of about 0.4 μm, a prodigious increase in light scattering sets in.

The scattered light is measured with an optical dark field arrangement somewhat similar to that used by Gucker *et al.* (*5*) for a colloidal particle counter. The image of an annular mask *M* acting as virtual light source, is projected on a complementary mask *M′*, which in our case consists of an aluminum tube with an optically polished surface cut at 45°. Thus, photomultiplier *PM1* receives the scattered light, whereas the direct light is conducted through a glass fiber cable into *PM2*. The photomultipliers are a matched pair and receive their voltage from an operational power supply. The circuitry, by controlling the high voltage, keeps the signal from *PM2* constant. Thus, the signal from *PM1* represents the scattered light, undistorted by attenuation, while the change in high voltage is very closely proportional to the absorbance, as has been experimentally demonstrated with neutral density filters.

Figure 2 gives a comparison between the theoretical and experimental light scattering behavior of the growing water droplets. A typical oscilloscope picture obtained with air-conditioned laboratory air is shown in the inset. Trace 1 represents the pressure change; trace 2, the scattered light; trace 3, the first derivative of trace 2; and trace 4, the absorbance (downward).

Light scattering by particles larger than about 0.1 μm is explained by Mie's theory (*6*); we used a Sigma 5 computer and light scattering functions (*7*) derived from Mie's mathematical formalism. The angular scattering co-

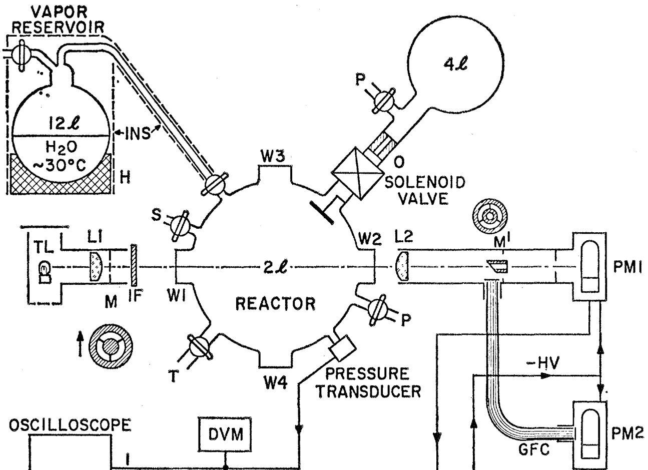

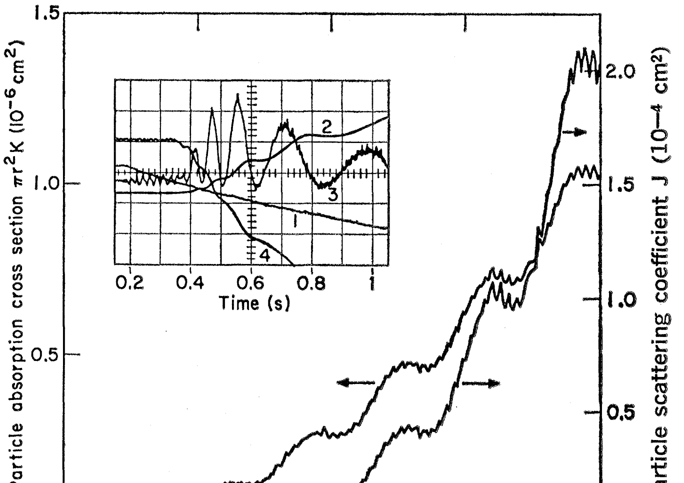

Fig. 1 (left). Schematic diagram of the Argonne condensation nucleus discriminator. *H*, heating mantle; *INS*, heat insulation; *P*, outlets to vacuum pump; *O*, variable orifice; *S*, sample inlet; *T*, tank air inlet; *W1* to *W4*, silica windows; *TL*, tungsten iodine lamp; *L1* and *L2*, lenses; *IF*, interference filter; *M*, annular mask; *M′*, complementary mask; *GFC*, glass fiber cable; *PM1* and *PM2*, photomultipliers; *HV*, high voltage; *VM*, voltmeter; *DVM*, digital voltmeter. Fig. 2 (right). Mie scattering coefficient in the forward direction and particle absorption cross section for spherical water droplets at $\lambda = 433$ nm, as a function of droplet radius. (Inset) Oscilloscope picture of an expansion experiment on air-conditioned laboratory air; time is in seconds. (Trace 1) Pressure drop, 100 torr per large division; (trace 2) forward light scattering, relative units; (trace 3) rate of change of light scattering, relative units; (trace 4) absorbance, 0.02 unit per large division.

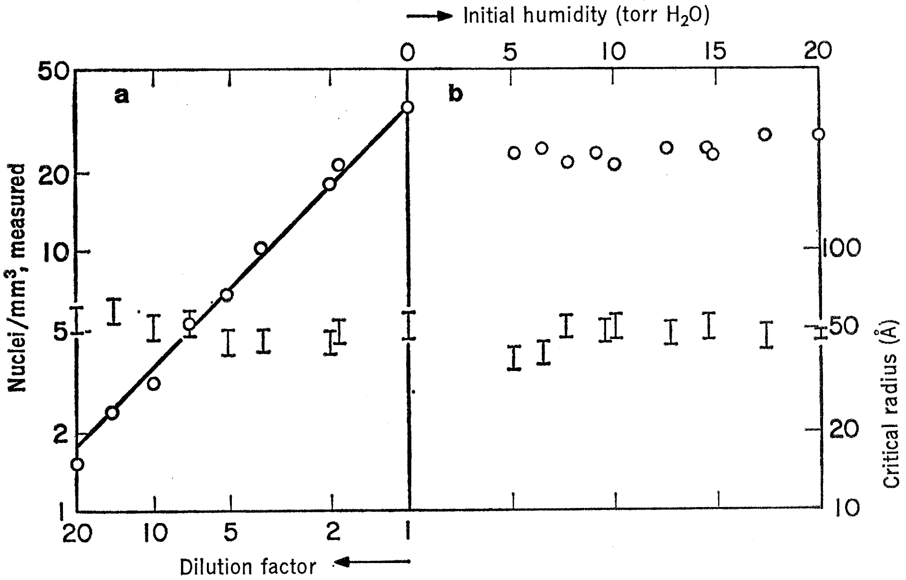

Fig. 3. Measured nucleus concentration, n, and critical radius, r_c, of sulfate aerosol as a function of dilution (a) and humidity (b). The ordinate scales are applicable for both halves of the figure. (Circles) Nucleus concentration; (I-bars) critical radius; (solid line) best-fitting 45° line. The error limits for r_c (length of the bars) were calculated from the uncertainties of the measured pressure drop, the humidity, and the temperature in the reactor.

efficient J for the scattering angle $\gamma = 180°$ (forward direction) and the absorption cross section $\pi r^2 K$ for spherical, nonabsorbing water droplets with an index of refraction of 1.34 were calculated as functions of the radius r for monochromatic, unpolarized light at the wavelength $\lambda = 433$ nm. The resulting curves are plotted in the main part of Fig. 2. The coefficients J and K are defined by the equations:

$$I_d = I_0 \exp(-n\pi r^2 K d) \qquad (1)$$

$$dI_s = I_d J n dV/X^2 \qquad (2)$$

where I_0 is the intensity of the incident light, I_d and I_s are the intensities of the direct and scattered light, n is the droplet concentration, d the path length, dV the scattering volume, and X the distance from dV.

With the aid of the calculated curves, we can assign a droplet radius to each of the steps in oscilloscope traces 2 and 4 (or the "Mie peaks" in trace 3) and thus plot a droplet growth function. By extrapolating the latter to the time axis, the beginning of droplet growth can be determined. From the pressure change at this point, the temperature drop and degree of supersaturation are obtained.

The relation between the critical radius r_c of a liquid droplet and the minimum supersaturation at which it can survive and grow, is given by (*8*):

$$r_c = 2M\sigma_L/\rho_L RT \ln(p/p_\infty) \qquad (3)$$

where M, σ_L, and ρ_L are the molecular weight, surface tension, and density of the liquid; R is the gas constant; p is the pressure of the supersaturated vapor; and p_∞ is the equilibrium vapor pressure at temperature T. Assuming that the condensation nucleus can be treated as a water droplet, we use Eq. 3 to calculate its size r_c. Although this method of calculating r_c for airborne particulate matter is generally accepted, Rich (*9*) has pointed out that r_c defined by Eq. 3 is "that radius of water drop which starts condensation at the same value of saturation as the unknown particle; but it should be observed that this probably is not the physical radius, even in the case of a spherical drop" (*10, 11*).

Unambiguous determination of r_c is only possible if the prevalent type of nucleus has a narrow size distribution. This is generally observed with laboratory air (see Fig. 2, inset). In the case of a bimodal distribution with a sufficient separation of the size groups it is sometimes possible to obtain reasonably reliable values for the two radii. For broad distributions only the maximum r_c can be estimated.

The concentration of nuclei, n, is calculated from the absorbance, A (displayed as trace 4 in the inset of Fig. 2) by using the formula

$$n = \frac{A_i \ln 10}{(\pi r^2 K)_i d} \qquad (4)$$

derived from Eq. 1. Here A_i is the absorbance measured at plateau i and $(\pi r^2 K)_i$ is the corresponding particle absorption cross section from Fig. 2. Because of the relatively large aperture of the complementary stops we find an increasing deviation between the observed and the calculated ratios of successive plateaus in the absorbance and, to a larger degree, in the scattering curves. However, values of n obtained from Eq. 4 for $i = 1$ and 2 always show good agreement (after correction for the expansion). For our air sample we obtain 19,160 ± 1,500 nuclei/cm³. Measurable light scattering can still be obtained for as few as 100 nuclei/cm³.

The reliability and reproducibility of the instrument was tested in a series of experiments. As the concentration of nuclei for both laboratory air and outside air varied rapidly, we produced a fairly constant stream of sulfate nuclei by irradiating a humidified air-SO_2 mixture with ^{90}Sr-^{90}Y beta rays (see also below). First we compared the instrument with a Gardner Associates counter (*12*), which was calibrated in the factory, at two different nucleus concentrations. Our instrument measured average values of 4.6×10^4 and 3.9×10^5 nuclei/cm³, the Gardner instrument 4.0×10^4 and 3.8×10^5 nuclei/cm³. Then we studied the effect of dilution and humidity on the measured values of n and r_c. In the first series of experiments (Fig. 3a) we diluted our sulfate aerosol up to 20 times with filtered tank air but maintained a constant humidity of 20 torr of H_2O at about 24°C by adding water vapor. With humidified tank air alone we obtained no measurable signal. The nucleus concentrations plotted in Fig. 3a were corrected for an observed drift of the value obtained for no dilution. The plot shows satisfactory proportionality between the measured and the calculated nucleus concentrations. Furthermore, dilution causes no significant variation of the measured r_c values displayed as vertical bars in Fig. 3b.

Humidity, too, has little or no effect on n and r_c as measured with our counter. In a series of experiments where the initial humidity was varied from 5 to 20 torr, gas samples with a constant nucleus concentration demonstrated no significant trend in either n or r_c (Fig. 3b). Since the expansion required for the beginning of droplet growth varies from 1.094 to 1.49 in these experiments and at the same time n and r_c remain constant, we conclude that the expansion is, in effect, an adiabatic one. The slight downward trend of n with decreasing humidity (increasing expansion) could be caused by increased turbulence producing an inhomogeneous distribution of the nuclei and increased losses to the wall during expansion.

Some conditions suitable for kinetic studies have been established. Sulfuric acid condensation nuclei readily form in a humid SO_2 atmosphere irradiated by ultraviolet light or ionizing radiations. Immediately after formation, the condensation nuclei possess a broad size distribution characterized by single, structureless scattering and light attenuation curves. However, the condensation nuclei soon coalesce and form larger particles with a much narrower size distribution, and reliable measurements of n and r_c can be made by the methods described above. The number concentration n is proportional to the time of irradiation up to particle concentrations of 4×10^5 cm^{-3}. This work was carried out with a 1-mc ^{90}Sr-^{90}Y beta-ray source, 10 torr of water vapor, an SO_2 concentration of 0.78 part per million (ppm), and 740 torr of filtered tank air. Under these conditions a large response is obtained and measurements can be made at the first absorbance level of Fig. 2.

Some exploratory studies have also been carried out to determine the usefulness of our instrument in reaction kinetics. Carbon monoxide and methane appreciably diminish the number of nuclei formed in beta-irradiated air containing 2.53 ppm of SO_2. At this stage we theorize that these organic compounds interfere with the oxidation of SO_2 by the OH radicals formed by the action of the beta rays on the air–water vapor system (*13*). This competition may be represented simply as:

$SO_2 + OH \rightarrow$ condensation nuclei
$CO + OH \rightarrow$ no condensation nuclei
$CH_4 + OH \rightarrow$ no condensation nuclei

Thus, by measuring the inhibition of nucleus formation by CO and CH_4 separately, we can deduce the rate constant ratio $k(CO + OH)/k(CH_4 + OH)$ (*14*). At 25°C we obtain a ratio of 22.9, a result that compares favorably with Greiner's value of 16.8 (*15*), obtained by kinetic spectroscopy at 300°K. Thus a new method for measuring relative rate constants for reactions of OH radicals may be developed with the Argonne condensation nucleus discriminator. Similar laboratory studies could be carried out with other radicals such as H, HO_2, and O as well as with ozone and singlet O_2.

Condensation nucleus counters are widely employed in atmospheric research (*3, 4, 10*), and because of their high sensitivity in detecting particles with radii in the range 10 to 200 Å they are being used to study the minute chemical changes involved in gas-to-particle conversion reactions (*16*). With the improved size discrimination and absolute counting features of our instrument, we believe that it will find general application in physical and chemical studies on condensation nuclei.

EDWIN J. HART
KLAUS H. SCHMIDT
KEELATHUR N. VASUDEVAN*
Chemistry Division, Argonne National Laboratory, Argonne, Illinois 60439

References and Notes

1. V. J. Shaefer, testimony before the Senate Subcommittee on Public Works, 91st Congress, 2nd Session, 16 to 18 March 1970; published in *Third Annual Report* (Atmospheric Sciences Research Center, State University of New York, Albany, 1970), p. 1.
2. L. D. Carver, *Ind. Res.* **13**, 41 (August 1971); A. Hogan, in *Third Annual Report* (Atmospheric Sciences Research Center, State University of New York, Albany, 1970), p. 36; L. W. Pollak and T. Murphy, *Geofis. Pura Appl.* **25**, 44 (1953).
3. G. F. Skala, *Anal. Chem.* **35**, 702 (1963).
4. K. T. Whitby, B. Y. H. Lin, R. B. Husar, N. J. Barsic, *J. Colloid Interface Sci.* **39**, 136 (1972).
5. F. T. Gucker, C. T. O'Konski, H. B. Packard, J. N. Pitts, Jr., *J. Amer. Chem. Soc.* **69**, 2422 (1947).
6. G. Mie, *Ann. Phys. Leipzig* **25**, 377 (1908).
7. National Bureau of Standards, *Tables of Scattering Functions for Spherical Particles* (Government Printing Office, Washington, D.C., 1949), p. ix; R. O. Gumprecht and C. M. Sliepcevich, *Tables for Light-Scattering Functions for Spherical Particles* (Univ. of Michigan Press, Ann Arbor, 1951), p. x; *Tables of Riccati-Bessel Functions for Large Arguments and Orders* (Univ. of Michigan Press, Ann Arbor, 1951), p. xii.
8. B. J. Mason, *Discuss. Faraday Soc.* **30**, 20 (1960).
9. T. A. Rich, *Geofis. Pura Appl.* **31**, 60 (1955).
10. The critical radius depends on the nature of the particles. Equation 3 applies to homogeneous nucleation and to water-insoluble particles. In water-soluble particles the activity of the solution must also be taken in account (*11*). In the absence of these data and, indeed, in the case of air, with no knowledge of the nucleating species, we use Eq. 3 without correction for particle activity.
11. K. G. Vohra and P. V. N. Nair, *J. Atmos. Sci.* **28**, 280 (1971).
12. Gardner Associates, Schnectady, New York.
13. Beta-ray energy absorbed by O_2 and N_2 in moist air produces OH radicals within 10^{-8} second even at H_2O pressures of 0.2 torr. (S. Gordon and W. A. Mulac, unpublished results.
14. E. J. Hart and K. H. Schmidt, *Radiat. Res.*, in press.
15. N. R. Greiner, *J. Chem. Phys.* **46**, 2795 (1967).
16. K. G. Vohra, K. N. Vasudevan, P. V. N. Nair, *J. Geophys. Res.* **75**, 2951 (1970).

17. Work performed under the auspices of the U.S. Atomic Energy Commission.

* Present address: Department of Physics, Illinois Institute of Technology, Chicago 60616.

16 October 1972; revised 9 March 1973

■

Genetic Polymorphism of Proline-Rich Human Salivary Proteins

Abstract. *In randomly collected saliva samples from 120 Caucasians, 79 Blacks, and 40 Chinese, three phenotypes were observed by electrophoresis in alkaline slab polyacrylamide gels. The proteins showing polymorphism were identical with four previously characterized proline-rich proteins. Inheritance is controlled by two autosomal codominant alleles. The gene frequencies were for Caucasians,* $Pr^1 = 0.73$, $Pr^2 = 0.27$; *for Blacks,* $Pr^1 = 0.80$, $Pr^2 = 0.20$; *for Chinese,* $Pr^1 = 0.84$, $Pr^2 = 0.16$.

A new genetic polymorphism among a set of four proline-rich proteins from parotid saliva is described. These proteins, designated as proteins I, II, III, and IV, have been isolated and partially characterized (*1*). They display chemical features which in certain respects resemble collagen, and in other ways have a similarity to enamel protein. These proteins are notably rich in proline, glycine, glutamine, and asparagine (*1*) and have a marked affinity for hydroxyapatite (*2*). Our finding of a common genetic polymorphism among proline-rich salivary proteins should stimulate the search for a possible relation between genetic variation of these proteins and oral disease (*3*). The high frequency of this polymorphism among all the populations studied indicates that it may be useful for other types of genetic research, especially linkage studies.

Electrophoresis of concentrated parotid saliva in alkaline slab polyacrylamide gels and staining with a 3,3′-dimethoxybenzidine–hydrogen peroxide solution revealed a series of rapidly migrating negative-staining bands on an opaque or brown background (*4, 5*).

These proteins exhibit unusual characteristics when stained with amido black and Coomassie blue (*1*). In a collection of random samples from different racial groups, three patterns were recognized among four of these proteins (Fig. 1: I, II, III, and IV). Proteins I and II in region A and proteins III and IV in region B show parallel changes in the different samples. Negative-staining proteins other than I, II, III, and IV (Fig. 1) were